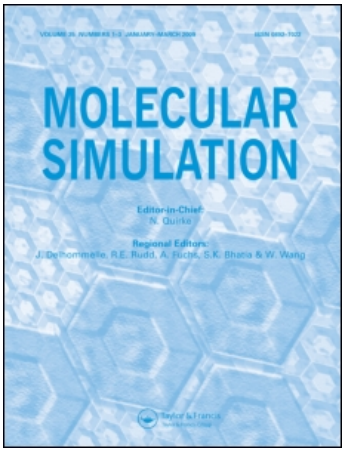

Molecular Simulation
Publication details, including instructions for authors and subscription information:
http://www.informaworld.com/smpp/title~content=t713644482

Structure and dynamics of Ti-Al-H compounds in Ti-doped $NaAlH_4$

G. K. P. Dathara[a]; D. S. Mainardi[a]
[a] Institute for Micromanufacturing, Louisiana Tech University, Ruston, USA

To cite this Article Dathara, G. K. P. and Mainardi, D. S.(2008) 'Structure and dynamics of Ti-Al-H compounds in Ti-doped $NaAlH_4$', Molecular Simulation, 34: 2, 201 — 210
To link to this Article: DOI: 10.1080/08927020801930596
URL: http://dx.doi.org/10.1080/08927020801930596

Molecular Simulation
Vol. 34, No. 2, February 2008, 201–210

Taylor & Francis
Taylor & Francis Group

Structure and dynamics of Ti–Al–H compounds in Ti-doped $NaAlH_4$

G.K.P. Dathara and D.S. Mainardi*

Institute for Micromanufacturing, Louisiana Tech University, Ruston, USA

(Received 15 December 2007; final version received 19 January 2008)

Structure and stability of pristine and modified $NaAlH_4$ are first investigated using density functional theory (DFT) with plane-wave basis and PW91 functional. Vacancy and Ti-dopant effects in the sodium alanate bulk, (0 0 1) surface, and on-top (0 0 1) surface are then studied considering Na and interstitial lattice sites. Calculated substitution energies of Ti-doped (0 0 1) $NaAlH_4$ surfaces have shown almost equal probability of substitution at both lattice and interstitial sites. Ti–Al–H complexes are formed depending on the accessible AlH_4 groups around the Ti dopant. $TiAl_2H_7$ and $TiAl_2H_2$ complexes are found after geometry optimising doped-$NaAlH_4$ surface models. Their stability and dynamics over time at 423 and 448 K are investigated using periodic density functional molecular dynamics (DFT-MD) simulations. Results have shown increased association of Al and H with the complexes as time evolves. DFT-MD simulations show evolution from $TiAl_2H_7$ to $TiAl_5H_7$ as time and temperature increase in case of Ti dopant at Na surface site ($Ti \rightarrow S_{Na}$), and evolution from $TiAl_2H_2$ to $TiAl_3H_6$ at 423 K and $TiAl_3H_7$ at 448 K in case of Ti dopant on-top of the interstitial surface site ($Ti \rightarrow T_I$) with time.

Keywords: titanium; dopant; sodium alanate; metal hydrides; diffusion

1. Introduction

Targets set by the United States Department of Energy (DoE) for the development of on-board storage materials include systems able to achieve a gravimetric hydrogen density of about 9 wt% and volumetric density $\sim 81\ kg/m^3$ by 2015, including reversibility of hydrogen storage and release [1]. Complex metal hydrides are considered promising hydrogen storage materials due to their potential for achieving the gravimetric and volumetric hydrogen storage densities set by the DoE [2]. However, the practical use of complex metal hydrides in transportation applications is currently limited by their slow hydrogen absorption/desorption kinetics and high temperatures for hydrogen release.

Sodium aluminium hydride (sodium alanate, $NaAlH_4$) is one of the most investigated light metal hydrides due to its high hydrogen content and ability to speed up the reversible hydrogen absorption/desorption kinetics by addition of transition metal dopants, such as zirconium, vanadium and in particular titanium through the incorporation of Ti-containing compounds, such as $TiCl_3$ [3–7]. Two hypotheses have been drawn from those studies. Either titanium forms a catalytically active complex with components of $NaAlH_4$, or it performs lattice substitutions with Na [7–10] or Al [11] or both [12]. When the formation of NaCl due to the titanium salt used is possible, experiments show that Na sites are preferred by Ti dopant over Al sites since the overall energy required to replace Na by Ti is less compared to the energy required to replace Al by Ti [13]. This observation is consistent with the experimental work by Fichtner et al. [10], who reported preference of Ti dopants for Na over Al sites. In a recent XANES and EXAFS work by Baldé et al. [14] interstitial sites and sites on the hydride surface are reported to be the preferred ones for titanium. In spite of these observations, the preferred sites for Ti dopant in the $NaAlH_4$ lattice are still debated in the literature.

Besides preferred sites for Ti dopants, resulting compounds from ball milling with titanium salts and cycling at various temperatures are also extensively investigated, since they are believed to be responsible for the improved hydrogen desorption kinetics by Ti-doped $NaAlH_4$. DFT studies by Lee et al. [15] suggested that Na and Al substitution by Ti in sodium alanates is unfavourable; however, the formation of $TiAl_3$ is thermodynamically favourable. Experimental EXAFS studies by Chaudhuri et al. [16] also showed the formation of stable intermetallic species resembling $TiAl_3$. Brinks et al. [17,18] have showed the formation of a solid $Al_{1-x}Ti_x$ solution with $x \sim 0.07$ after cycling at 160°C. Haiduc et al. [19] found an hcp-Ti(Al) solid solution after doping with $TiCl_3$, and an XRD-amorphous phase when $NaAlH_4$ was doped with $Ti(OBu)_4$. These authors have

*Corresponding author. Email: mainardi@latech.edu

ISSN 0892-7022 print/ISSN 1029-0435 online

DOI: 10.1080/08927020801930596
http://www.informaworld.com

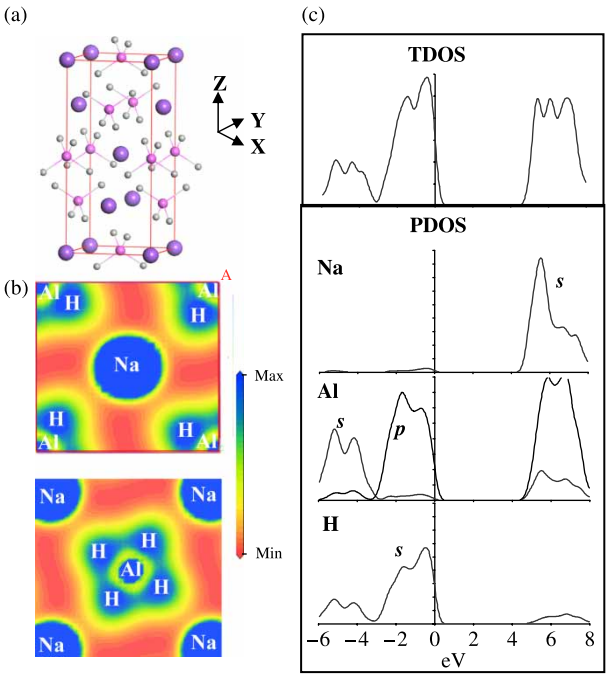

Figure 1. (a) Calculated ground state structure of $NaAlH_4$ unit cell atom colours: purple-sodium, magenta-aluminium and grey-hydrogen. (b) Electron density maps of slices parallel to *X* and *Y* axes in $NaAlH_4$ unit cell. The highest (max) and lowest (min) electron densities are blue and red, respectively. (c) Total (TDOS) of $NaAlH_4$ and partial (PDOS) density of states of Na, Al and H in $NaAlH_4$.

also observed that the composition of those Ti compounds is temperature dependent. At temperatures up to 175°C an amorphous Al–Ti alloy is formed, while at temperatures higher than 200°C intermetallic phases of the Al_xTi form are present. Baldé et al. [14] also observed the formation of crystalline $TiAl_3$ after heat treatment at 475°C and amorphous $TiAl_3$ at 225°C. From all these studies, the presence of one or more phases of Ti–Al compounds is expected to tune the thermodynamics and kinetics of Ti-doped sodium alanates. Moreover, the surface morphology of the doped particles may also affect the kinetics of hydrogen desorption [20,21]. In spite of all experimental and theoretical investigations on this topic, the basic role of titanium dopant in the formation of key intermetallics for improved hydrogen kinetics by sodium alanates is still unknown.

In this work, lattice structure and stability upon Ti doping at different bulk, surface and interstitial sites in $NaAlH_4$ are first investigated using DFT with plane-wave basis. Formation of Ti–Al–H compounds are then identified and their dynamics investigated using periodic density functional molecular dynamics (DFT-MD) simulations in order to understand the temperature effect on titanium atom diffusion in the doped-$NaAlH_4$ following chemisorption.

2. Methodology

Generalised gradient approximation (GGA) calculations within the DFT formalism is used in this paper for the study of structure and stability of pristine and modified sodium alanates. The Perdew and Wang (PW91) functional [22] and plane-wave basis (PW) set with valence electrons described by Vanderbilt ultra-soft pseudopotentials (USPP), is employed in all the calculations as implemented in the module CASTEP® [23] of the Materials Studio® software by Accelrys, Inc. [24]. DFT using plane wave basis set with valence electrons described using USPP or projector augmented wave are commonly used to determine the structure and energetics of $NaAlH_4$ and Ti doped $NaAlH_4$ [11,13,15,16,25–31]. All the geometry optimisation calculations performed are spin-unpolarised. The cutoff energy is 400 eV with convergence criteria set at 2.0×10^{-5} eV atom^{-1}, and a k-point separation of 0.05 Å^{-1} on unit cells and super cells. Electron density maps as well as total and partial density of states plots are calculated for the systems under investigation.

In order to study the temperature effect on titanium atom diffusion in Ti doped-$NaAlH_4$ following chemisorption, DFT-MD simulations are conducted as implemented in CASTEP at 423 and 448 K. In DFT-MD, each step performs a classical molecular dynamics step with forces computed at the aforementioned GGA/PW91/PW-USPP theory level. NVT ensemble dynamics is used in this calculations considering a Nose–Hoover thermostat with a chain length of 7 (number of thermostats coupled to maintain the target temperature in the ensemble). With the wavefunction extrapolation scheme implemented in CASTEP®, usually time steps in the order of 1 femtosecond (1 fs = 10^{-15} s) provide good numerical stability and conservation of the constant of motion comparable to force field based molecular dynamics methods [32]. The time-step used for the simulations is 2 fs, and results from 2-ps simulations are reported here. The mean signed deviation in the constant of motion observed in our calculations is in the order of 4.5 kJ/mol.

3. Results

3.1 Structure of pristine $NaAlH_4$

A sodium alanate unit cell (Figure 1(a)) is built according to its tetragonal structure, which belongs to the *I*41/*a* space group (#88) with sodium, aluminium and hydrogen atoms occupying the 4(*a*), 4(*b*) and 16(*f*) Wyckoff positions, respectively, with $x_H = 0.2662$, $y_H = 0.6084$ and $z_H = 0.0442$ [31]. Calculated DFT ground state $NaAlH_4$ lattice parameters and bond lengths (Table 1) are well in agreement with the values reported by Hauback et al. [33] from their neutron diffraction experiments.

Table 1. Calculated structural parameters of $NaAlH_4$ unit cell.

	Calc. (Å)	Expt.[a] (Å)
Lattice parameters	$a = b = 4.982$	$a = b = 4.98$
	$c = 11.149$	$c = 11.15$
Na–Al	3.523	3.52
Al–H	1.612	1.63

[a] From [32].

The $NaAlH_4$ electron density maps are shown in Figure 1b, where a coloured scale is used to quantify the electron density within the lattice (highest, blue and lowest, red). According to this scale, not only valence but also core electrons densities are represented and therefore, all atomic species are coloured blue. Figure 1(b) shows higher electron density within the AlH_4 groups than between Na atoms and AlH_4 complexes as expected for this crystal. From the $NaAlH_4$ total (TDOS) and partial (PDOS) density of states plots (Figure 1c), it can be noticed that the valence band of $NaAlH_4$ is mainly formed by contributions from the *s* orbital of hydrogen and the *p* orbital of aluminium, while the electronic states containing the *s* orbital of sodium are in the conduction band. The calculated band gap of the $NaAlH_4$ cell is 4.9 eV, which compares well with the value of 4.8 eV reported by Ozolins et al. [31].

3.2 *Structure of modified $NaAlH_4$*

In this section, vacancy and Ti-dopant effects in the sodium alanate bulk (Figure 2(a)), (0 0 1) surface (Figure 2(b)) and on-top (0 0 1) surface (Figure 2(c)) are studied considering Na and interstitial sites. Structure and energetics of pristine and modified $NaAlH_4$ models are presented and discussed in terms of bond lengths, TDOS, PDOS and cohesive (E_{coh}), substitution (ΔE_{subst}) and titanium-addition (ΔE_{add}) energies. Cohesive energy is defined as the difference between the energy of the total system and the sum of the individual atomic energies. The substitution energy per atom of Na by X (= vacancy or Ti), ΔE_{subst}, is defined by Equation (1)

$$\Delta E_{subst} = \frac{E_{coh}(X\mathrm{Na}_{n-1}\mathrm{Al}_n\mathrm{H}_{4n}) - E_{coh}(\mathrm{Na}_n\mathrm{Al}_n\mathrm{H}_{4n})}{N}, \quad (1)$$

where N is the total number of atoms in the model, $n = 16$ for bulk substitution and $n = 8$ for surface substitution, respectively, according to the lattice models used. The energies per atom resulting from titanium-addition to interstitial and on-top surface sites, ΔE_{add}, is defined by Equation (2).

$$\Delta E_{add} = \frac{E_{coh}(\mathrm{TiNa}_8\mathrm{Al}_8\mathrm{H}_{32}) - E_{coh}(\mathrm{Na}_8\mathrm{Al}_8\mathrm{H}_{32})}{N}. \quad (2)$$

3.2.1 *Bulk models*

A ($2 \times 2 \times 1$) supercell consisting of 16 $NaAlH_4$ units ($Na_{16}Al_{16}H_{64}$) with $N = 96$ atoms is built by extending the tetragonal $I4_1/a$ sodium alanate cell twice along the '*a*' and '*b*' lattice dimensions. A Na atom inside the $NaAlH_4$ bulk occupying the B_{Na} site (Figure 2(a)) is chosen to be removed (vacancy creation) or substituted by a Ti dopant. Hence, lattice models representing a vacancy at this Na bulk site ($0 \rightarrow B_{Na}$) and Ti in B_{Na} site ($Ti \rightarrow B_{Na}$) are constructed and geometry optimised using plane wave DFT techniques. Changes in structure and energetics due to vacancy ($0 \rightarrow B_{Na}$) and Ti dopant in $NaAlH_4$ bulk ($Ti \rightarrow B_{Na}$) are discussed in detail in our earlier paper [34]; however, the main conclusions are summarised here.

Calculations show that the lattice structure is preserved in both cases ($0 \rightarrow B_{Na}$ and $Ti \rightarrow B_{Na}$), however, changes in bond lengths are seen mainly in the $Ti \rightarrow B_{Na}$ case (Table 2). The first row in Table 2 represents the average B_{Na} nearest neighbouring Al–X bond lengths, where X = Na (pristine), 0 ($0 \rightarrow B_{Na}$) and Ti ($Ti \rightarrow B_{Na}$); that is either the B_{Na} site is occupied by Na, left vacant or replaced by the Ti dopant. The native

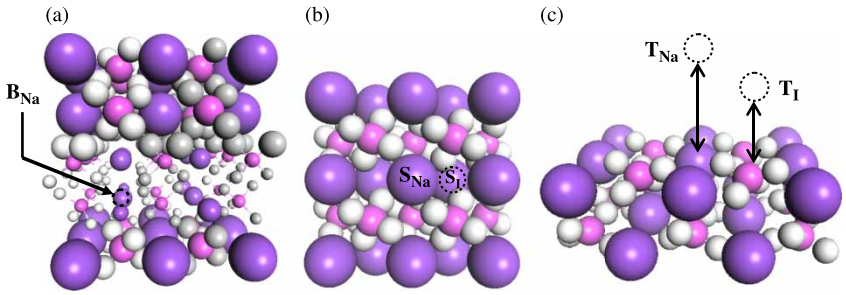

Figure 2. Models of $NaAlH_4$ with different sites tested for Ti dopants. (a) Bulk: Na lattice site "B_{Na}" (b) Surface: Na lattice site "S_{Na}" and interstitial site "S_I" in the surface of $NaAlH_4$ and (c) sites "T_{Na}" and "T_I" on the $NaAlH_4$ surface. Purple, magenta and white/grey represent Na, Al and H atoms, respectively.

Table 2. Bond distances between Al and H with vacancy (0) and Ti dopant in bulk Na site (B_{Na}).

Bond lengths (Å) \ Species in B_{Na} site	Na	0	Ti
Al	3.523	–	3.219
H	2.410	–	2.028
Al–H (nearest neighbours)	1.612	1.583–1.626	1.599–1.671
Na–Al (nearest neighbours)	3.523	3.477	3.400
Al–H (average, other than nearest neighbours)	1.612	1.611	1.606

Al–Na bond length 3.523 Å; however, when Na is substituted by Ti dopant the new bond length, Al–Ti, is decreased by ~0.3 Å. The second row in Table 2 represents the average B_{Na} nearest neighbouring H–X bond lengths (X = Na, 0, Ti). The calculated H–Ti bond length is ~2 Å, which is 0.4 Å shorter than the corresponding Na–H in pristine sodium alanate.

The third and fourth rows in Table 2 show values for the B_{Na} nearest neighbouring Al–H and Na–Al bond lengths. These Al–H bond lengths increased in the order of 0.06 Å for Ti → B_{Na}, whereas a slight increase in this distance (by 0.014 Å) is found when 0 → B_{Na}. Significant decrease in the Na–Al bond lengths (~0.12 Å) compared to the Al–H distances is found when titanium substitutes Na in B_{Na}, where as the decrease in Na–Al distance when Na is substituted by a vacancy is in the order of 0.05 Å when compared to the pristine lattice. Finally, the fifth row in Table 2 represents the average Al–H bond lengths other than the B_{Na} nearest neighbouring distances in the AlH_4 groups. Relative to the Al–H bond lengths in pristine $NaAlH_4$, the corresponding distances decrease by 0.005 Å in the Ti → B_{Na} case and remain almost the same when 0 → B_{Na}.

All the structural differences found mainly when Ti → B_{Na} can be attributed to the difference in atomic radii of sodium (1.86 Å) and titanium (1.47 Å) atoms. The presence of titanium dopants replacing the native sodium sites B_{Na} results in a decrease of the lattice parameters, and shows changes in the distances between sodium and hydrogen as well as aluminium and hydrogen. Elongation and therefore weakening of Al–H bond in the presence of a Ti at B_{Na} is observed and supported by calculations of density of states and electron density maps from the changes in the overall electronic structure [34]. Change in the electronic structure indicates possible formation of intermetallics such as Ti–Al and Ti–H compounds. From the cohesive energy calculations (Table 3) is seen that Ti → B_{Na} is 1.88 eV more stable than the pristine $NaAlH_4$, and the later is 6.85 eV more stable than the case in which a vacancy is created at B_{Na} (0 → B_{Na}).

In order to get insights on Ti diffusion into the $NaAlH_4$ bulk, surface models of sodium alanate are built and Ti-substituted surface Na as well as Ti addition in surface interstitial sites, and on-top Na and interstitial surface site models are investigated and discussed in the next section.

3.2.2 *Surface and on-top surface models*

The (0 0 1) $NaAlH_4$ surface is investigated in this work. This surface is found to be closely packed and has the least surface energy compared to the $NaAlH_4$ (1 0 0), (1 0 1) and higher order crystallographic planes such as (1 1 0) and (1 1 2) [13]. In order to facilitate modelling of Ti doping on and above the (0 0 1) $NaAlH_4$ surface, a two-layer slab exposing the (0 0 1) $NaAlH_4$ crystallographic surface with a vacuum thickness of 5 Å is built by cleaving the (2 × 2 × 1) supercell to expose the (0 0 1) crystal surface (Figure 3). The total system then consists of 8 $NaAlH_4$ units ($Na_8Al_8H_{32}$) containing $N = 48$ atoms.

Table 3. Cohesive energy relative to pristine system, E_{coh}*, Ti-addition energy, ΔE_{Ti} and substitution (vacancy (0) → Na and Ti → Na) ΔE_{subst} energy.

Site	Species in site	System	E_{coh}* (eV)	ΔE_{Ti} (eV atom^{-1})	ΔE_{subst} (eV atom^{-1})
B_{Na}	Na	$Na_{16}Al_{16}H_{64}$	0.00		
	0	$Na_{15}Al_{16}H_{64}$	−6.85		−0.07
	Ti	$TiNa_{15}Al_{16}H_{64}$	1.88		0.02
S_{Na}	Na	$Na_8Al_8H_{32}$	0.00		
	0	$Na_7Al_8H_{32}$	−6.68		−0.14
	Ti	$TiNa_7Al_8H_{32}$	3.23		0.07
S_I	Ti	$TiNa_8Al_8H_{32}$	6.58	0.13	
T_{Na}	Ti	$TiNa_8Al_8H_{32}$	3.89	0.08	
T_I	Ti	$TiNa_8Al_8H_{32}$	3.46	0.07	

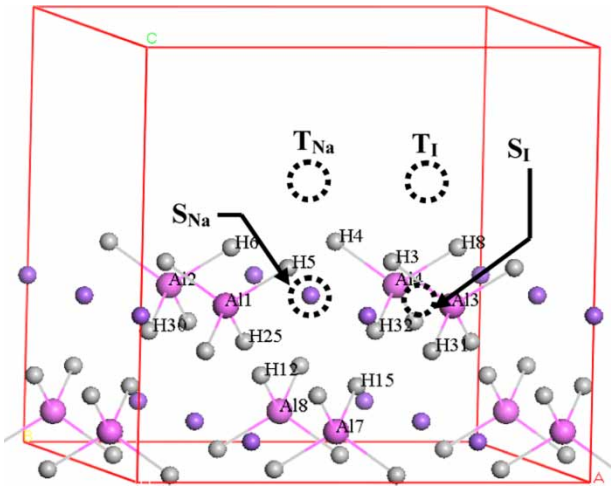

Figure 3. Representative model for (0 0 1) $NaAlH_4$ surface with atoms labelled for reference. Test sites on surface (S_{Na} and S_I) as well as on top surface (T_{Na} and T_I) are shown.

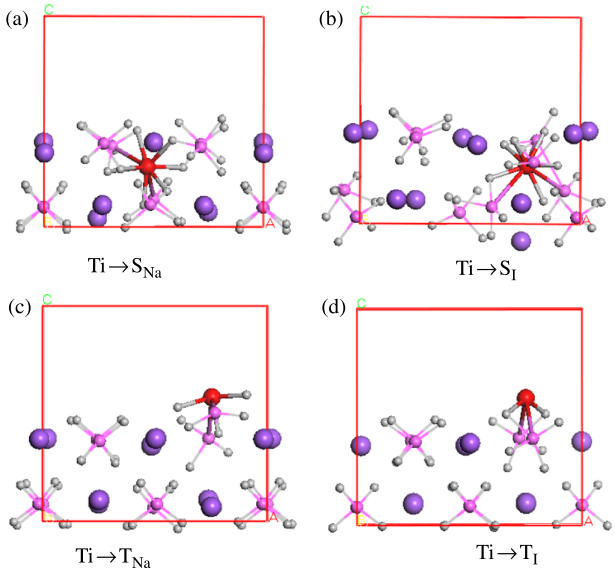

Figure 4. Optimised models of Ti doped $NaAlH_4$ surfaces with Ti dopant occupying different test sites ((a) S_{Na}, (b) S_I, (c) T_{Na} and (d) T_I).

Six different models are constructed to investigate vacancy creation and effects of Ti dopants. Test sites for substitution/addition of point defects (vacancy, Ti dopant) are designated as 'S_{Na}' (Na lattice site in top layer) (Figure 2(b)), 'S_I' (interstitial site between two Na lattice sites and two Al lattice sites in top layer) (Figure 2(b)), 'T_{Na}' (site on top of S_{Na}) and 'T_I' (site on top of S_I) (Figure 2(c)). Hence, the six models considered are Na → S_{Na} (pristine), 0 → S_{Na} (vacancy creation on the surface at S_{Na} site), Ti → S_{Na} (Ti-substituted Na at S_{Na}), Ti → S_I (Ti added to the interstitial surface S_I site), Ti → T_{Na} (Ti placed on-top the surface S_{Na} site), and Ti → T_I (Ti placed on-top the surface interstitial S_I site).

Constructed models are geometry optimised and ground state conformations are shown in Figure 4 for the models considering titanium. The Ti dopant (red) at S_{Na}, Ti → S_{Na} model (Figure 4(a)), settles between the surface and sub-surface layers forming bonds with hydrogen and aluminium atoms in surrounding accessible AlH_4 groups. This creates a distortion in the crystal lattice mainly due to the difference between ionic radii of titanium and sodium atoms. From the Ti local environment in the Ti → S_{Na} model it is observed that the Ti atom coordinates to seven H atoms at distances in the 1.81–1.97 Å range, and two aluminium atoms at distances in the 2.6–2.7 Å range. Up to eight hydrogen and five aluminium atoms have been found at distances from the Ti dopant in the 1.84–2.00 Å and 2.61–3.40 Å ranges, respectively, in this case [13]. Since typical Ti–Al and Ti–H bond lengths in TiAl and TiH compounds such as $TiAl_3$ and TiH_2 are in the 2.7–2.9 Å [35] and in the order of 1.92 Å [35], respectively, the possible formation of a Ti–Al–H complex ($TiAl_2H_7$) is predicted in our calculations. In such complex, the calculated average distance between Ti dopant and the two nearest neighbouring Al atoms (Al2 and Al8) is 2.65 Å, and the seven nearest neighbouring hydrogen atoms is 1.9 Å in very good agreement with bond lengths in typical TiAl and TiH compounds.

The optimised Ti → S_I model (Figure 4(b)) shows that Ti dopant resides in the interstitial space right below the surface and forms a Ti–Al–H complex with neighbouring lattice Al and H atoms. From the Ti dopant local environment in this model it is observed that the Ti coordinates to five H and three aluminium atoms at distances in the 1.81–1.90 and 2.51–2.93 Å (average 2.75 Å) ranges, respectively. Hence, the possible formation of a $TiAl_3H_5$ complex is seen in the Ti → S_I case.

After placing the Ti dopant on-top the surface Na site, T_{Na}, (Ti → T_{Na} model, Figure 4(c)), it migrates to the T_I site during the geometry optimisation calculation. After optimisation is complete, the Ti dopant resides above the crystal surface and therefore, little distortion is introduced in the $NaAlH_4$ lattice structure. In this case, a more localised Ti–Al–H complex is formed. The Ti atom is coordinated to three hydrogen and two aluminium atoms at distances in the 1.74–1.86 and 2.50–2.75 Å ranges, suggesting the possible formation of a $TiAl_2H_3$ compound. Similarly in the case of Ti → T_I model (Figure 4(d)), the Ti dopant resides above the crystal surface and therefore, little distortion is introduced in the $NaAlH_4$ lattice structure. A $TiAl_2H_2$

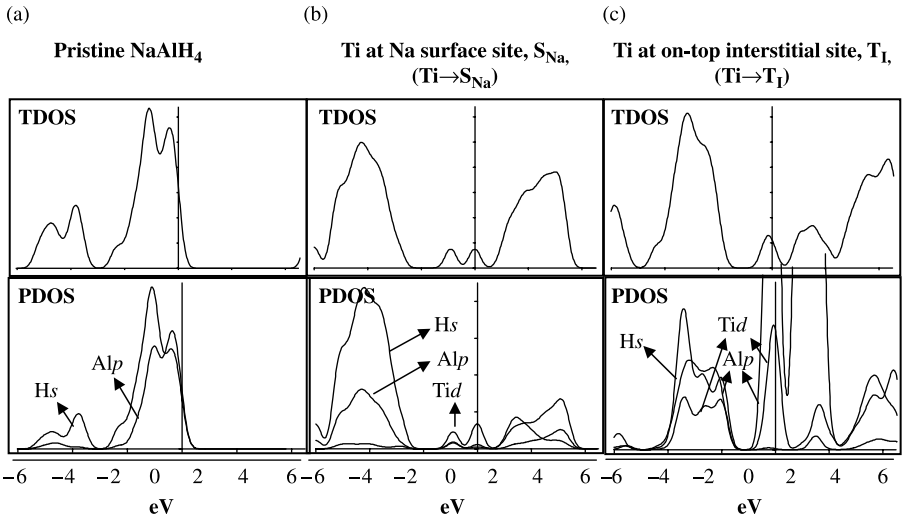

Figure 5. TDOS and PDOS plots from optimised (a) pristine, (b) Ti → S_{Na} and (c) Ti → T_I models.

compound seems to form with Ti–H bond length of 1.73 Å and Ti–Al bond lengths in the 2.74–2.77 Å range.

From the cohesive energy calculations (Table 3), the cohesive energies of models Ti → S_{Na}, Ti → S_I, Ti → T_{Na} and Ti → T_I are higher than to corresponding to pristine $NaAlH_4$ surface model, and therefore possible. In order to analyse the preferred sites for titanium dopants on the (0 0 1) $NaAlH_4$ surface, the energy required to perform Ti → S_{Na}, Ti → S_I, Ti → T_{Na} and Ti → T_I with respect to the pristine case is calculated. Hence, the substitution energy Equation (1) for the Ti → S_{Na} model and titanium-addition energies Equation (2) for the Ti → S_I, Ti → T_{Na} and Ti → T_I models are computed. Calculations show that the energy required for such substitution/addition is Ti → S_{Na} ≈ Ti → T_I < Ti → T_{Na} < Ti → S_I (Table 3). The difference between the energy required for Ti → S_{Na} and Ti → T_I is 0.003 eV $atom^{-1}$, while the energy required for Ti → S_I is substantially higher than the corresponding one in the other three cases. Since the energy required for Ti → S_{Na} and Ti → T_I is less compared to others, these two sites (S_{Na} and T_I) and probably T_{Na} would be preferred by the Ti dopants over S_I. However, occupation of the S_I sites by Ti dopant would be also possible at elevated temperatures due to increased supplied energy as well as diffusion of the dopants on the surface and/or into the lattice.

3.2.3 *Density of states*

Similar DOS plots are obtained for the optimised Ti → S_{Na} and Ti → T_I models (Figure 5). Looking at the contributions from different atomic orbitals of Ti, Al and H species in doped-$NaAlH_4$ it is possible to elucidate the particular Ti–Al–H complexes that form when Ti → S_{Na} and Ti → T_I in $NaAlH_4$ take place. A shift in the Fermi level towards the conduction band is seen with introduction of Ti dopant in the lattice at both, S_{Na} and T_I sites. The calculated band gaps are, respectively, 1.00 and 0.93 eV in the Ti → S_{Na} and Ti → T_I models. The pristine $NaAlH_4$ TDOS plot (Figure 5(a)) shows contributions from the *s* orbital of hydrogen and the *p* orbital of aluminium. The TDOS and PDOS of the Ti → S_{Na} model (Figure 5(b)) show that the energy states found right below the Fermi level are mainly formed by contributions from the *d* orbital of titanium, while in the case of Ti → T_I (Figure 5(c)), they are formed by contributions from the *d* orbital of Titanium and *p* orbital of aluminium.

In Ti → S_{Na} model, Ti is coordinated to two aluminium and seven hydrogen atoms. Moreover, since the individual Al–H bond lengths increase with respect to the bonds in the pristine lattice (bond lengths in the AlH_4 groups are increased by 0.03–0.20 Å), the possible formation of a $TiAl_2H_7$ complex is suggested.

In the case of Ti → T_I, Ti is coordinated to two aluminium and two hydrogen atoms, and since the individual Al–H bond lengths in the AlH_4 groups are increased (by 0.20 Å), the possible formation of a $TiAl_2H_2$ complex is predicted. Hydrogen atoms H3 and H8 (Figure 3) that were previously bonded to aluminium in pristine $NaAlH_4$, have shown no significant interaction with Al after optimisation of the Ti → T_I model; Al–Ti and Al–H average bond distances are 2.75 and 1.77 Å in the $TiAl_2H_2$ complex, respectively.

From these studies we can conclude that the energy required to free the hydrogen atoms bound to AlH_4 groups in pristine $NaAlH_4$ is decreased due to introduction of titanium, resulting in the possible

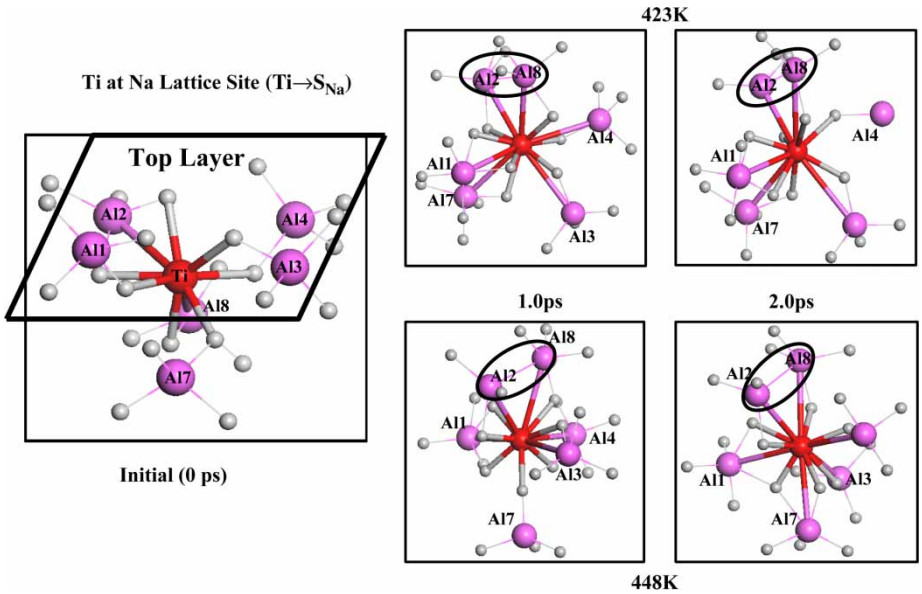

Figure 6. Snapshots showing the time evolution of $TiAl_2H_7$ complexes in Ti → S_{Na} model at two time steps from DFT-MD simulations at 423 and 448 K. Atom colours: Red (Ti), magenta (Al) and grey/white (H). Hydrogen atoms encircled in black represent number of hydrogen atoms associated with the complex as a result of hydrogen hopping from AlH_4 groups other than that are shown in the picture.

formation of $TiAl_2H_7$ and $TiAl_2H_2$ complexes with hydrogen atoms shared between Al and Ti. DOS of Ti doped $NaAlH_4$ of Ti–Al–H complexes, illustrates a possible catalytic role of Ti, i.e. lowering the formation energy of AlH_3-type species and therefore, the barrier for H_2 desorption.

Our DFT results show that the complex observed in Ti → T_I model is a precursor to the complexes observed in Ti → S_I and Ti → T_{Na} models when subjected to elevated temperatures. Hence, further analysis is concentrated on the Ti–Al–H complexes that are believed to form in the Ti → S_{Na} and Ti → T_I models. Thus, in next section, the dynamics of $TiAl_2H_7$ and $TiAl_2H_2$ complexes over time at different temperatures is discussed and insights into the diffusion of Ti dopants in the $NaAlH_4$ lattice are presented.

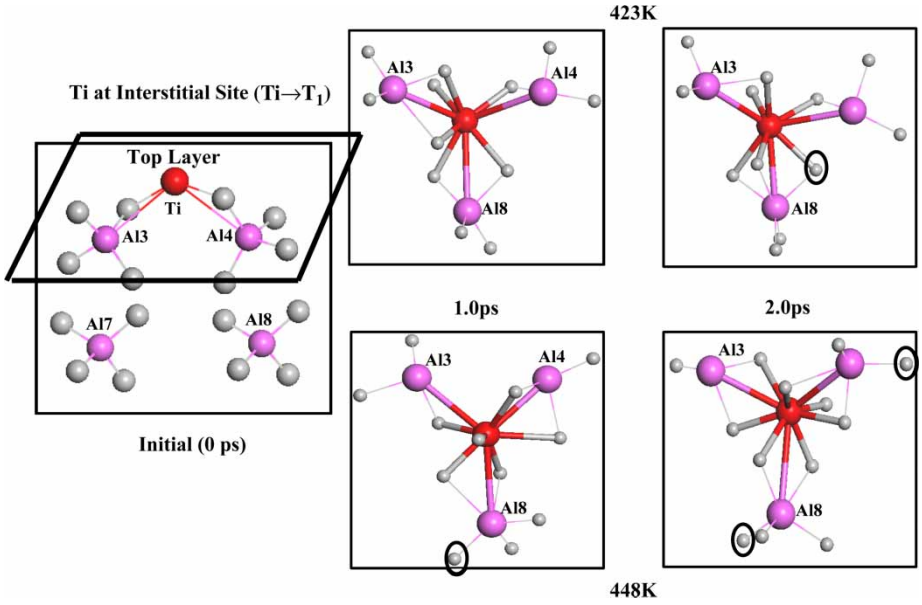

Figure 7. Same as Figure 6 for $TiAl_2H_2$ in Ti → T_I model.

3.3 Dynamics of Ti-doped $NaAlH_4$

The time evolution of $TiAl_2H_7$ (Figure 6) and $TiAl_2H_2$ (Figure 7) complexes after formed in $Ti \rightarrow S_{Na}$ and $Ti \rightarrow T_I$ models at 423 and 448 K are investigated with DFT-MD simulations. Initial total environment around dopant is shown in Figure 4a ($TiAl_2H_7$) and 4b ($TiAl_2H_2$), and subsequent pictures show the local complex environments at three different time intervals (0, 1 and 2 ps) at both temperatures in Figures 6 and 7, respectively. Different views are taken in Figures 6 and 7 with respect to Figure 4 for better visualisation of the complexes and association of aluminium atoms. In Figure 7 the atoms circled black represent hydrogen atoms that hop from neighbouring AlH_4 groups to dopant accessible AlH_4 groups.

From the results of DFT-MD simulations of $Ti \rightarrow S_{Na}$ model at 423 and 448 K, it is noticed that the Ti dopant settles between surface and subsurface layers and no further diffusion into the lattice is seen. The neighbouring six AlH_4 groups are drawn towards the Ti dopant, and increased association of aluminium atoms as well as hydrogen atoms with Ti is found after dynamics (Figures 6 and 7).

After 1 ps at 423 K, the number of aluminium atoms coordinating with titanium in the complex increase from two (at distances in the 2.6–2.7 Å range) to five (at distances in the 2.6–2.7 Å range). The number of hydrogen atoms (seven) coordinating with titanium are at distances in the 1.76–2.02 Å range, resulting in the possible formation of $TiAl_5H_7$ complex at 423 K after 1 ps. Besides the formation of a Ti–Al–H complex, Al–Al association (with a 2.97 Å bond length) is also seen from the DFT-MD results at this temperature. After 2 ps, no significant changes are observed in the complex except for the rearrangement of the Ti–Al–H complex with a Al2–Al8 bond length of 2.62 Å. All the other bond lengths remain unaltered.

When temperature is set to 448 K, no significant changes in the $TiAl_5H_7$ complex is seen over time. Rearrangement of Al and H atoms in this complex is however observed, but the number of hydrogen and aluminium atoms associated with the complex remains unaltered. The Al–Al distance reduces to 2.78 and 2.46 Å after 1 and 2 ps, respectively, at this temperature.

In the case of $Ti \rightarrow T_I$ model where the $TiAl_2H_2$ complex is formed, diffusion of dopant into the $NaAlH_4$ lattice is seen with temperature (Figure 7) through the top layer with final settling between surface and sub-surface layers. At 423 K and after 1 ps (Figure 7), the number of aluminium atoms coordinating with Ti dopant (at distances in the 2.57–2.76 Å range) increases from two to three and the number of coordinating hydrogen atoms (at distances in the 1.74–2.00 Å range) increase from two to six, resulting in the formation of a $TiAl_3H_6$ complex. After 2 ps at 423 K, the complex remains unchanged with rearrangement of associated aluminium and hydrogen atoms. Hydrogen hopping from one AlH_4 group to another is seen after 2 ps at 423 K.

At 448 K and after 1 ps, the Ti–Al–H complex is the same as the one found after 2 ps at 423 K ($TiAl_3H_6$). After 2 ps at this temperature, the coordinating aluminium atoms remain the same (at an average distance of 2.73 Å from Ti), and coordinating hydrogen atoms increased from six to seven (at distances from Ti in the 1.69–1.97 Å range), resulting in the formation of a $TiAl_3H_7$ complex.

The results on $Ti \rightarrow T_I$ at different temperatures suggest that the formed complexes are possible after diffusion of Ti dopants from the surface into the lattice, penetrating through the interstitial site on the surface (S_I). From this result it is expected that the Ti dopant placed initially at a T_{Na} site would diffuse on the surface and penetrate through the interstitial site based on aforementioned discussions.

4. Discussion

When compared to the presence of dopants in bulk and surface, $NaAlH_4$ with Ti dopants in bulk tends to be less stable than the case of $NaAlH_4$ with Ti dopants on its surface, as observed from the differences in cohesive energies of the different models presented here. From the cohesive energy point of view, $Ti \rightarrow S_I$ is the most stable conformation possible. Looking at the energy required to introduce dopants in the $NaAlH_4$ lattice through titanium substitution and titanium addition energies (ΔE_{subst} and ΔE_{add}), bulk substitution is favourable followed by $Ti \rightarrow S_{Na}$ and $Ti \rightarrow T_I$. The first step for the dopant before substitution at the lattice site would be to adsorb on the surface and diffuse into the lattice. Hence, the preferred sites for Ti dopants to adsorb after initial mechanochemical milling process may be estimated by comparing the possible sites for surface substitution. From the constructed models to simulate the (0 0 1) $NaAlH_4$ surface doping, two possibilities of substitution at Na lattice site ($Ti \rightarrow S_{Na}$) as well as substitution on top of interstitial site between two Na and two Al atoms ($Ti \rightarrow T_I$) have equal probability since the energy required to do that is similar in both cases.

From DFT simulations it is found that the Ti dopant prefers to settle between the surface and subsurface layers in case of $Ti \rightarrow S_{Na}$ and $Ti \rightarrow S_I$ models, and on the surface in case of $Ti \rightarrow T_{Na}$ and $Ti \rightarrow T_I$ models. Optimised configurations with the Ti dopant placed at possible sites on the $NaAlH_4$ surface (T_{Na}, S_I and T_I) result in the same model after simulating dynamics at elevated temperatures. Formation of $TiAl_2H_7$ and

$TiAl_2H_2$ depend upon the accessible AlH_4 groups from the Ti local environment. These complexes are shown to weaken the Al–H bonds in AlH_4 complexes since the hydrogen atoms that were previously bonded only to an aluminium atom are now shared between the Ti dopant and aluminium atom. This effect would help in lowering the required energy for hydrogen desorption from the doped-$NaAlH_4$ lattice, facilitating hydrogen desorption by forming a multi-atomic complex.

Ti dopants replacing Na atoms would result in a complex with Ti surrounded by all the adjacent six AlH_4 groups in case of the $NaAlH_4$ lattice structure. This Ti dopant surrounded by six Al atoms can be interpreted as the reported Ti–Al solid solution observed after mechanochemical milling of $NaAlH_4$ and $TiCl_3$ [19]. Since the Ti dopants on the (0 0 1) $NaAlH_4$ surface also have equal probability, a more localised complex is seen in Ti $\rightarrow$ T_I, since Ti dopant has access to only two AlH_4 groups.

From the dynamics of the formed Ti–Al–H complexes at different temperatures, it is seen that Ti dopant prefers to reside between surface and subsurface layers with no further diffusion into the lattice irrespective of the surface model under consideration. After that diffusion process, mobility of AlH_4 groups is observed towards the Ti dopant, resulting in association of more Al atoms with Ti dopants over time at different temperatures. After 2 ps simulation, Ti forming bonds with five Al atoms and six hydrogen atoms in case of Ti $\rightarrow$ S_{Na} and three aluminiums and six hydrogen atoms in case of Ti $\rightarrow$ T_I is seen. The Ti–Al–H complex in the case of Ti $\rightarrow$ S_{Na} model seems like a precursor to the phase with atomic Ti dispersed in aluminium. Complex observed in case of Ti $\rightarrow$ T_I model seems like a precursor to the $TiAl_3$ phase, since association of Ti with three Al atoms is seen with a high covalent character in the formed Ti–Al bonds.

5. Conclusions

In this work, the role of titanium dopant in the formation of key intermetallics for improved hydrogen kinetics of sodium alanates is investigated using DFT with plane-wave basis and PW91 functional. The $NaAlH_4$ lattice structure and stability upon Ti-substituted bulk and surface Na sites, as well as Ti addition in surface interstitial sites and Ti on-top Na and interstitial surface sites are investigated. Equal probability of Ti dopant substitution at both lattice and interstitial Na sites in the (0 0 1) $NaAlH_4$ surface is found from substitution energies calculations. The composition of Al and H in the observed Ti–Al–H complexes depends on the accessible AlH_4 groups around the Ti dopant, and $TiAl_2H_7$ and $TiAl_2H_2$ are found to form after geometry optimisation calculations. Periodic DFT-MD simulations are then conducted in order to understand the temperature effect on titanium atom diffusion on the doped-$NaAlH_4$ following chemisorption at 423 and 448 K. Results have shown the existence of the observed Ti–Al–H complexes as well as increased association of Al and H with the complexes as time evolves at both temperatures. The complexes observed after geometry optimisation represent the TiAl solid solution observed after ball milling of $TiCl_3$-doped $NaAlH_4$, and the complexes at elevated temperatures represent precursors to amorphous $TiAl_3$ and atomic Ti dispersed in aluminium, making this study consistent with experimental observations.

Acknowledgements

Financial support from the US Department of Energy under grant DoE/BES DE-FG02-05ER46246 and the Louisiana Optical Network Initiative (LONI) Institute is grateful acknowledged. Support for computational resources for both software and hardware through the Louisiana Board of Regents, contract LEQSF(2007-08)-ENH-TR-46 and the National Science Foundation Grant No. NSF/IMR DMR-0414903 is also thankfully acknowledged.

References

[1] DoE, *Hydrogen Posture Plan* (2004). Available at www.doe.gov.
[2] M. Jacoby, *Filling up with hydrogen*, C & EN (2005), pp. 42–47.
[3] B. Bogdanović et al., *Improved hydrogen storage properties of Ti-doped sodium alanate using titanium nanoparticles as doping agents*, Adv. Mater. 15 (2003), pp. 1012–1015.
[4] B. Bogdanović and M Schwickardi, *Ti-doped alkali metal aluminium hydrides as potential novel reversible hydrogen storage materials*, J. Alloys Compd. 253 (1997), pp. 1–9.
[5] B. Bogdanović et al., *Metal-doped sodium aluminium hydrides as potential new hydrogen storage materials*, J. Alloys Compd. 302 (2000), pp. 36–58.
[6] D.L. Anton, *Hydrogen desorption kinetics in transition metal modified $NaAlH_4$*, J. Alloys Compd. 356–357 (2003), pp. 400–404.
[7] K.J. Gross, E.H. Majzoub, and W. Spangler, *The effects of titanium precursors on hydriding properties of alanates*, J. Alloys Compd. 356–357 (2003), pp. 423–428.
[8] D. Sun et al., *X-ray diffraction studies of titanium and zirconium doped $NaAlH_4$: elucidation of doping induced structural changes and their relationship to enhanced hydrogen storage properties*, J. Alloys Compd. 337 (2002), pp. L8–L11.
[9] J. Íñiguez et al., *Structure and hydrogen dynamics of pure and Ti-doped sodium alanate*, Phys. Rev. B (2004), pp. 0601011–0601014.
[10] M. Fichtner et al., *Nanocrystalline alanates—phase transformations, and catalysts*, J. Alloys Compd. 404–406 (2005), pp. 732–737.
[11] O.M. Løvvik et al., *Density functional calculations of Ti-enhanced $NaAlH_4$*, Phys. Rev. B 054103 (2005), pp. 054101–054110.
[12] M.E. Arroyo y de Dompablo and G Ceder, *First principles investigations of complex hydrides AMH_4 and A_3MH_6 (A = Li, Na, K, M = B, Al, Ga) as hydrogen storage systems*, J. Alloys Compd. 364 (2004), pp. 6–12.
[13] T. Vegge, *Equilibrium structure and Ti-catalyzed H_2 desorption in $NaAlH_4$ nanoparticles from density functional theory*, Phys. Chem. Chem. Phys. 8 (2006), pp. 4853–4861.

[14] C.P. Baldé et al., *Active Ti species in $TiCl_3$-doped $NaAlH_4$. Mechanism for catalyst deactivation*, Phys. Chem. C 111 (2007), pp. 2797–2802.
[15] E.K. Lee, Y.W. Cho, and K. Yoon, Ab initio *calculations of titanium solubility in $NaAlH_4$ and $Na3AlH_6$*, J. Alloys Compd. 416 (2006), pp. 245–249.
[16] S. Chaudhuri et al., *Understanding the role of Ti in reversible hydrogen storage as sodium alanate: a combined experimental and density functional theoretical approach*, J. Am. Chem. Soc. 128 (2006), pp. 11404–11415.
[17] H.W. Brinks et al., *Synchrotron x-ray and neutron diffraction studies of $NaAlH_4$ containing Ti additives*, J. Alloys Compd. 376 (2004), pp. 215–221.
[18] H.W. Brinks et al., *Synchrotron x-ray studies of $Al_{1-y}Ti_y$ formation and Re-hydriding inhibition in Ti-enhanced $NaAlH_4$*, J. Phys. Chem. B 109 (2005), pp. 15780–15785.
[19] A.G. Haiduc et al., *On the fate of the Ti catalyst during hydrogen cycling of sodium alanate*, J. Alloys Compd. 393 (2005), pp. 252–263.
[20] V. Bérubé et al., *Size effects on the hydrogen storage properties of nanostructured metal hydrides: a review*, Int. J. Energy Res. 31 (2007), pp. 637–663.
[21] T.A. Dobbins et al., *Ultrasmall-angle X-ray scattering (USAXS) studies of morphological trends in high energy milled $NaAlH_4$ powders*, J. Alloys Compd. 446–447 (2007), pp. 248–254.
[22] J.P. Perdew and Y. Wang, *Accurate and simple analytic representation of the electron-gas correlation energy*, Phys. Rev. B 45 (1992), pp. 13244–13249.
[23] M.D. Segall et al., *First-principles simulation: ideas, illustrations and the CASTEP code*, J. Phys. Cond. Matt. 14 (2002), pp. 2717–2743.
[24] Accelrys, *Materials Studio®* (2006).
[25] A.J. Du, S.C. Smith, and Q. Lu, *Role of charge in destabilizing AlH_4 and BH_4 complex anions for hydrogen storage applications:* Ab initio *density functional calculations*, Phys. Rev. B 74 (2006), pp. 1934051–1934054.
[26] C. Moysés Araújo et al., Vacancy-mediated hydrogen desorption in $NaAlH_4$, Phys. Rev. B 72 (2005), pp. 165101–165106.
[27] J. Liu and Q Ge, *A first-principles analysis of hydrogen interaction in Ti-doped $NaAlH_4$ surfaces: Structure and energetics*, J. Phys. Chem. B 110 (2006), pp. 25863–25868.
[28] S. Chaudhuri and T. Muckerman, *First-principles study of Ti-catalyzed hydrogen chemisorption on an Al surface: a critical first step for reversible hydrogen storage in $NaAlH_4$*, J. Phys. Chem. B 109 (2005), pp. 6952–6957.
[29] S. Li, P. Jena and R Ahuja, *Effect of Ti and metal vacancies on the electronic structure, stability, and dehydrogenation of Na_3AlH_6: supercell band-structure formalism and gradient-corrected density-functional theory*, Phys. Rev. B 73 (2006), pp. 2141071–2141077.
[30] V. Ozolins, E.H. Majzoub, and J. Udovic, *Electronic structure and rietveld refinement parameters of Ti-doped sodium alanates*, J. Alloys Compd. 375 (2004), pp. 1–10.
[31] T. Arias, M.C. Payne, and D. Joannopoulos, Ab initio *molecular dynamics: analytically continued energy functionals and insights into iterative solutions*, Phys. Rev. Lett. 69 (1992), pp. 1077–1080.
[32] B.C. Hauback et al., *Neutron diffraction structure determination of $NaAlD_4$*, J. Alloys Compd. 358 (2003), pp. 142–145.
[33] G.K.P. Dathara and S. Mainardi, *Modeling Effects of Titanium Dopants on Hydrogen Adsorption/desorption Kinetics by Sodium Alanates*, AIChE 2007 Annual Meeting, Salt Lake City, UT, 2007.
[34] P. Norby and N. Christensen, *Preparation and structure of Al_3Ti*, Acta Chem. Scan. A 40 (1986), pp. 157–159.
[35] P.E. Irving and A. Beevers, *Some metallographic and lattice parameter observations on titanium hydride*, Met. Trans. 2 (1971), pp. 613–615.